Numerical Methodology for Determining the Energy Losses in Auxiliary Systems and Friction Processes Applied to Low Displacement Diesel Engines

Sofia Orjuela Abril [1], Jhan Piero Rojas [2] and Eder Norberto Flórez [3],*

[1] Programa de Administración de Empresas, Universidad Francisco de Paula Santander, Avenida Gran Colombia No. 12E-96 Barrio Colsag, San José de Cúcuta 540001, Colombia; sofiaorjuela@ufps.edu.co
[2] Programa de Ingeniería Civil, Universidad Francisco de Paula Santander, Avenida Gran Colombia No. 12E-96 Barrio Colsag, San José de Cúcuta 540001, Colombia; jhanpierorojas@ufps.edu.co
[3] Facultad de Ingeniería, Universidad Francisco de Paula Santander, Sede el Algodonal Vía Acolsure, Ocaña-Norte de Santander 546551, Colombia
*   Correspondence: enflorezs@ufpso.edu.co; Tel.: +577-569-00-88

check for updates

Abstract: The problem of climate change and the reduction of fossil fuels has motivated the development of research focused on improving the efficiency of internal combustion engines. This research proposes a methodology based on mathematical models to determine the energy losses caused by auxiliary systems and friction processes in the engine. Therefore, models are proposed for calculating the energy losses in fuel injection, lubrication, and cooling system. In the same way, models are proposed for the energy losses due to friction in the piston, valve train, and bearings. Experimental tests are carried out on a single-cylinder diesel engine under different operating conditions to validate the proposed models. The results showed that the energy losses of the fuel injection, lubrication, and coolant system are equal to 0.61%, 0.30%, and 0.31% of the chemical energy of the injected fuel. In the case of the energy losses by friction processes, the piston, valve train, and bearings represent 5.47%, 1.34%, and 1.85% of the fuel energy, respectively. Additionally, the proposed model allows estimating the minimum lubrication film present in the piston, valve train, and bearings, which in the particular case of the present study were 0.63 μm, 0.10 μm, and 0.57 μm, respectively. In general, the methodology developed in the present work stands as a robust tool to evaluate the modifications and/or designs of auxiliary systems and friction processes to reduce the energy losses and protect the system from wear caused by lubrication problems. Additionally, the methodology allows evaluating the effect of different types of fuels on the lubrication conditions of the piston and the crankshaft bearings.

Keywords: auxiliary systems; energy losses; friction; hydrodynamic; lubrication; tribological performance

1. Introduction

Currently, internal combustion engines (ICE) are used in various economic activities, such as industrial processes, agriculture, electricity generation, and transportation [1–4]. Power generation through ICEs is of utmost importance for interconnected areas and to maintain a reliable operation that accounts for energy fluctuations and shortage on a grid line. The use of generators powered by ICE increases progressively every year [5]. Despite the advantages of ICEs, the activities that involve their use are responsible for between 15% and 18% of global CO_2 emissions [6,7]. This percentage tends to increase due to the globalized growth of economic activities [8]. In order to minimize the environmental impact, international organizations and governments have agreed to set strict levels of emission control for ICE [9]. In order to reduce ICE emissions, the implementation of different

post-treatment systems has been investigated, among which it is possible to highlight particle filters, selective catalytic reduction, and the catalytic converter [10–12]. However, the structure of the engines used for electricity generation limits the use of systems such as catalytic converters and exhaust gas recirculation [5]. Additionally, the installation of these systems causes high back pressures in the engine exhaust system. Therefore, greater pumping work is required, which produces an increase in fuel consumption [13,14]. As a result, it is necessary to implement alternative strategies to reduce the emissions of ICEs for electric power generation.

The reduction of pollutants in ICEs can be achieved by reducing fuel consumption, which is directly related to the energy efficiency of the engine. Efficiency in ICEs is reduced by mechanical losses, which significantly reduces the useful power of the engine. Mechanical losses are the consequence of energy losses in the pumping system, friction processes, and the energy necessary for the movement of engine components [15]. Therefore, one way to improve ICE efficiency is by reducing energy losses associated with the friction processes.

Friction losses account for approximately 12% of fuel energy. The sources of friction losses are located in the interactions between the cylinder liner and the piston skirt, the camshaft, and the bearings. Based on the prominent contribution of friction losses, different investigations have been carried out to minimize energy losses through different strategies such as oil system heating [16], low viscosity oil [17,18], smooth contact surfaces [19], and coating implementation [20,21].

Another alternative proposed for reducing friction losses is the development of mathematical models that allow quantifying and determining the origin of the energy loss associated with friction [22]. This type of model can be useful to improve the design of critical components such as the piston, the compression rings, the camshaft, and the bearings [23]. Dowson et al. [24] developed a one-dimensional model to estimate friction-associated losses in engines. The model used considers the movement of the elements to calculate the friction produced in the bearings. Dubois and Ocvirk [25] built a model to quantify friction losses in the piston mechanism. Taraza and Henein [26] implemented a mathematical model based on the Stribeck diagram.

Different tribological investigations indicate the importance of mechanical losses caused by friction processes and auxiliary systems. Furuhama and Sasaki [27] evaluated the lubrication performance in the contact between the piston rings and the cylinder liner. Tian [28] pointed out that tribological behavior plays an important role in the wear of the components and the variation of the lubrication film.

Over the years, the complexity of the models has increased since they are used to quantify the losses in specific areas of the engine. Liu et al. [29] studied the influence of surface texture on the lubrication performance between compression rings and cylinder liners. The study was carried out by applying a mixed lubrication model to evaluate the tribological behavior with the presence of spherical dimples in the cylinder liner. Similarly, Avan et al. [30] developed a tribological model to study the influence of the design of the piston rings on the energy losses produced by the contact in the cylinder liner and the piston. The model was used to estimate the thickness of the lubrication film and friction under different lubrication conditions. Jocsak et al. [31] evaluated the influence of different surface parameters on the cylinder liner. The analysis was performed through the implementation of non-Gaussian probability density functions, which were unified with the Greenwood and Tripp roughness contact model and the standard piston-ring friction model. Allmaier et al. [32] studied the thermodynamic behavior of the bearings using an isothermal elastohydrodynamic simulation model. The model was used to calculate the frictional power losses in the sleeve bearings. Likewise, Sander et al. [33] analyzed the mixed lubrication in plain bearings using experimental and numerical approaches. The study focused on the influence of the properties of non-Newtonian lubricants and the piezoviscous effect on power losses due to friction processes in bearings for different dynamic load conditions.

The ICE valve train is another mechanism that has been investigated to reduce friction losses. The strategies used involve the use of different surface textures between the cam-tappet and cam-roller connections [34]. In general, the estimation of the friction forces for this type of mechanism is carried

out using the Hertz contact model. Currently, there are different models focused on calculating the thickness of the lubrication film between the follower and the cam lobe [35].

Apart from the individual analysis for the dynamic and lubrication characteristics in the engine's systems and components, different alternatives have been evaluated in relation to the type of fuel used. Specifically, the study centers on the exploration of biodiesel blends from edible and non-edible vegetable oil, microalgae, water emulsions, and the incorporation of additives such as hydrogen, metallic compounds, and hydroxy. In general, the main focus is to obtain a fuel mixture that guarantees optimal performance while reducing emissions. However, the effect of this type of alternative fuels on the lubrication characteristics is normally not taken into consideration.

Generally, the analysis of the mechanical losses in the engine is performed in specific sections of the engine [36,37], such as the piston assembly [38], bearings [18], and valve train [39]. This makes it difficult to apply in a specific engine study at different operating conditions. Additionally, the identification of potential damaging friction conditions, the quantification of global mechanical losses, and the risk of direct contact between surfaces are more complex when different engine subsystems are considered together.

The objective of this study is to determine the energy losses in the auxiliary systems and the engine friction processes through the development of a compound methodology that integrates the effects of fuel injection, lubrication, and cooling systems. Also, the proposed methodology accounts for the energy dissipated by friction in the piston, valve train, and bearings. The series of mathematical models allow determining the thickness of the lubrication film located on the piston, valve train, and crankshaft bearings. This work serves as a further step to close the knowledge gap regarding energy losses in ICEs while providing a robust tool to determine the impact of modifications in engine components and systems or even the type of fuel in the overall performance of the engine.

2. Energy Loss Models for Auxiliary Systems

The energy losses of an engine can be classified into two groups. The first group corresponds to losses due to friction processes, which occur due to the interactions present in the valve train, piston, and bearings. The second group is a consequence of the auxiliary systems of the engine due to the energy required for its operation. The latter corresponds to the fuel injection, lubrication, and cooling systems. The models used to calculate the energy consumption of the auxiliary systems are described below.

2.1. Fuel Injection System

The power of the pump used in fuel injection systems depends on the pressure drop in the common rail and the volumetric flow. Therefore, the energy consumed from the pump (E_{fuel}) is calculated by means of Equation (1).

$$E_{fuel} = \frac{P_{cr} \cdot \dot{V}_f}{\eta_f} \tag{1}$$

where $\dot{V}_f$ is the volumetric flow of fuel, P_{cr} the common rail pressure (i.e., is considered as the pressure drop of the fuel injection system) and η_f the efficiency of the fuel pump. The volumetric flow of fuel is defined by Equation (2).

$$\dot{V}_f = \frac{\dot{m}_f}{\rho_f} \tag{2}$$

where $\dot{m}_f$ and ρ_f are the mass flow and density of the fuel, respectively. Replacing Equation (2) in (1) determines the equation used to calculate the energy consumed by the fuel injection system, which is shown in Equation (3).

$$E_{fuel} = P_{cr} \cdot \left(\frac{\dot{m}_f}{\rho_f \cdot \eta_f} \right). \tag{3}$$

2.2. Lubrication System

The energy consumption of the oil pump is determined by Equation (4).

$$\dot{E}_{lub} = \frac{\Delta P_{lub} \cdot \dot{V}_{lub}}{\eta_{lub}} \tag{4}$$

where P_{lub} is the pressure drop across the lubrication pipe, $\dot{V}_{lub}$ is the volumetric flow of the lubricant and η_{lub} is the efficiency of the pump. The pressure drop in the lubrication pipe is determined by the Darcy–Weisbach equation, as shown in Equation (5) [40].

$$\Delta P_{lub} = \frac{8 \cdot f_{pipe}}{g \cdot \pi^2} \cdot \frac{L_{pipe}}{D_{pipe}^2} \cdot \dot{V}_{lub}^2 \tag{5}$$

where D_{pipe}, L_{pipe}, g, and f_{pipe} are the diameter of the pipe, the length of the pipe, gravity, and the friction factor of the pipe, respectively. f_{pipe} is calculated from the Moody formula [41], as shown in Equation (6):

$$f_{pipe} = 1.375 \times 10^{-3} \cdot \left[1 + \left(\frac{800 \cdot \dot{V}_{lub} \cdot \rho_{lub} \cdot r_{pipe} + \pi \cdot D_{pipe} \cdot \mu_{lub} \times 10^6}{4 \cdot \dot{V}_{lub} \cdot \rho_{lub}} \right)^{1/3} \right] \tag{6}$$

where μ_{lub}, ρ_{lub}, and r_{pipe} are the dynamic viscosity of the lubricant, the density of the lubricant, and the roughness of the pipe, respectively.

2.3. Cooling System

In the particular case of this study, the engine cooling system is carried out by means of a forced ventilation system caused by the presence of a fan. The calculation of the energy losses in this type of system can be defined as shown in Equation (7) [42].

$$\dot{E}_c = \tau \cdot N = \left(k \cdot N^2 \right) \cdot N \tag{7}$$

where N is the rotational speed of the engine, and k is the fan factor, which depends on the characteristic curve and the design of the blades.

A more direct alternative to calculating the energy losses in these systems is by measuring the electrical operating characteristics of the fan, as shown in Equation (8).

$$\dot{E}_c = V_s \cdot I \tag{8}$$

where V_s is the supply voltage and I is the electric current. In the case of having cooling systems using centrifugal pumps, it is possible to estimate the energy losses by applying the methodology shown in Section 2.2.

3. Energy Loss Models for Friction Processes

The models used to calculate the energy losses caused by friction processes, which occur due to the interactions present in the valve train, piston, and bearings, are described below.

3.1. Energy Losses in the Valve Train

The interaction between the follower and the cam produces contact friction $\left(F_{cf,v} \right)$, which is a consequence of the viscosity force due to the lubricant shear and the asperity [43,44]. Therefore, contact friction is defined by Equation (9).

$$F_{cf,v} = F_{ac,v} + F_{vf,v} \tag{9}$$

where $F_{ac,v}$ and $F_{vf,v}$ are the asperity contact force and viscous friction force, respectively. The asperity contact force ($F_{ac,v}$) is determined by the Equation (10):

$$F_{ac,v} = c_p l_c + \tau_{ss} A_a \tag{10}$$

where c_p, l_c, A_a, and τ_{ss} are the coefficient of the shear strength, load carried by the asperities, asperity area, and Eyring shear stress, respectively.

The load carried by the asperities (l_c) and asperity area (A_a) are determined by Equations (11) and (12) [45].

$$l_c = \sqrt{\frac{2 \cdot r_s}{r_a}} \cdot \left(\sqrt{\frac{16 \cdot \pi}{15}} \rho_a \cdot r_a \cdot r_s \cdot \sqrt{E_e \cdot H_c \cdot F_{5/2}} \right)^2 \tag{11}$$

$$A_a = H_c \cdot F_2 \cdot (\pi \cdot \rho_a \cdot r_a \cdot r_s)^2 \tag{12}$$

where r_s, r_a, ρ_a, E_e, and H_c are the composite surface roughness parameter, asperities radius of curvature, asperity density, effective elastic modulus, and Hertzian contact area, respectively.

The Hertzian contact area (H_c) is estimated by considering the contact between the follower and the cam as two cylinders. Therefore, H_c is calculated, as shown in Equation (13) [46]:

$$H_c = \left(\frac{24 \cdot r_e \cdot F_{n,v} \cdot w_{cam}^2}{\pi \cdot E_e} \right)^{\frac{1}{2}} \tag{13}$$

where r_e is the equivalent radius of curvature, w_{cam} is the cam width and $F_{n,v}$ is the normal force. The effective elastic modulus (E_e) is calculated by Equation (14).

$$\frac{1}{E_e} = \frac{1 - \vartheta_{foll}^2}{2 \cdot E_{foll}} + \frac{1 - \vartheta_{cam}^2}{2 \cdot E_{cam}} \tag{14}$$

where ϑ_{foll} and ϑ_{cam} are the Poisson's ratios of the follower and cam. E_{foll} and E_{cam} are young's modulus of the follower and cam.

Variables $F_{5/2}$ and F_2 are statistical functions dependent on the separation parameter (s_p), as shown in Equations (15) and (16) [43].

$$F_{5/2} = -0.93 + 0.61 s_p - 0.143 s_p^2 + 1.117 \times 10^{-2} s_p^3 + \frac{1.47}{e^{s_p}} \tag{15}$$

$$F_2 = -1.64 + 1.172 s_p - 0.31 s_p^2 + 0.3 \times 10^{-1} s_p^3 + \frac{2.26}{e^{s_p}} \tag{16}$$

The viscous friction force is determined from the model proposed by Goksem and Hargreaves [47], as shown in Equation (17).

$$F_{vf,v} = \frac{4.318 \cdot r_{cc} \cdot w_{cam}}{c_{pv}} \cdot \left(\frac{c_{pv} \cdot \mu \cdot v_e}{r_{cc}} \right)^{0.658} \cdot \left(\frac{F_{n,v}}{E_e \cdot r_{cc} \cdot w_{cam}} \right)^{0.0126} \tag{17}$$

where c_{pv}, r_{cc}, v_e and $F_{n,v}$ are the pressure viscosity coefficient, combined radius of curvature, entrainment velocity, and normal force, respectively.

The minimum thickness of the lubrication film (h_m) in the valve train is determined by means of Equation (18) [48].

$$h_m = 2.65 \cdot r_e \cdot \left(\frac{\mu \cdot v_e}{E_e \cdot r_e} \right)^{0.7} (c_{pv} \cdot E_e)^{0.54} \left(\frac{F_{n,v}}{E_e \cdot r_e} \right)^{-0.13} \tag{18}$$

Considering the above equations, the energy losses by contact friction in the valve train can be calculated by Equation (19) [49].

$$\dot{E}_{F_{cf,v}} = n_{ind} \cdot \left[\int_0^{2\pi} F_{ac,v}(\theta) \cdot v_c(\theta) \, d\theta \right] + n_{exh} \cdot \left[\int_0^{2\pi} F_{vf,v}(\theta) \cdot v_c(\theta) \, d\theta \right] \tag{19}$$

where v_c is the contact velocity, n_{ind} is the number of intake valves and n_{exh} is the number of exhaust valves.

3.2. Energy Losses in the Piston

To determine frictional energy losses in the piston, a configuration with three piston rings is considered, which consists of the top compression ring, the middle ring, and the lubrication control. This consideration is used since it is the most common configuration for internal combustion engines.

The friction forces in the piston rings depend on the interaction between the lining and the ring surface. Therefore, friction is closely related to the properties, thickness, and height of the lubrication film. Thus, the calculation of the friction force is made by considering the mechanics of the lubrication fluid. When constructing the model, a series of considerations are made:

- The inner diameter of the ring is considered rigid, so radial inertial forces are ignored.
- Flow processes are considered isothermal.
- The radial and tangential friction forces are calculated based on the Stribeck function.
- The Reynolds equation is used to determine the damping force.
- The flow of gas pressures is considered stationary.

To determine the relationship between the width, height, and thickness of the lubrication film on the surface of the piston rings, the Reynolds equation is used, which is described by Equation (20) [50].

$$\frac{\partial}{\partial y}\left(h^3 \cdot \frac{\partial p}{\partial y}\right) + \frac{\partial}{\partial x}\left(h^3 \cdot \frac{\partial p}{\partial x}\right) = 6 \cdot \eta\left(a \cdot \frac{\partial h}{\partial x} + v \cdot \frac{\partial h}{\partial y}\right) + 12 \cdot \mu \cdot \frac{dh}{dt}. \tag{20}$$

In the present study, the lubrication conditions between the cylinder liner and ring surface are determined as a function of the piston position. Therefore, the Reynolds equation can be reduced, as shown in Equation (21) [51]:

$$\frac{\partial}{\partial x}\left(h(x)^3 \cdot \frac{\partial p}{\partial x}\right) = 6 \cdot \eta\left(v \cdot \frac{\partial h(x)}{\partial x}\right) + 12 \cdot \mu \cdot \frac{dh(x)}{dt} \tag{21}$$

where v is the piston velocity, μ is the dynamic viscosity of the lubricant, p lubrication film pressure, and h is the thickness of the lubrication film, which is a function of the position on the piston.

The diagram of the forces applied to the piston rings is described in Figure 1.

$F_{fr,p}$ represents the frictional force produced between the ring face and the cylinder liner and is defined by Equation (22).

$$F_{fr,p,i} = F_{fr,s,i} + F_{fr,v,i} \tag{22}$$

where the subscript i can take the values of 1,2, and 3, which represent the top compression ring, the middle ring, and the lubrication control ring, respectively. $F_{fr,s}$ is the asperity friction force caused by the contact between the ring and the cylinder liner, and $F_{fr,v}$ the viscous friction force caused by the viscosity of the lubricant.
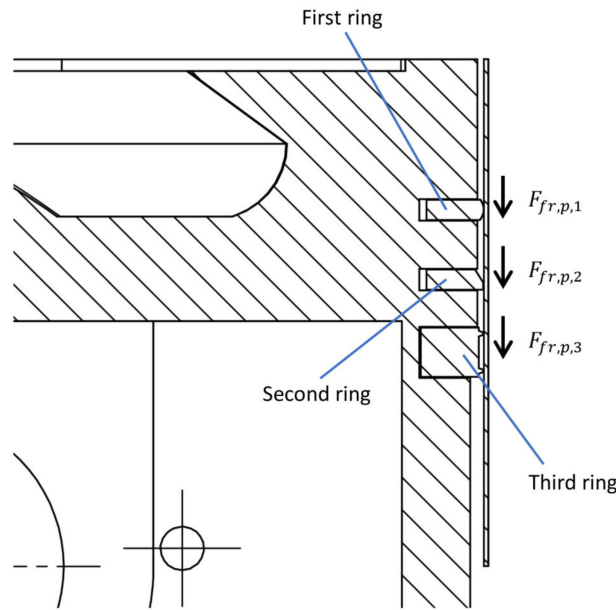
Figure 1. Frictional forces applied to piston rings.

The viscous friction force $\left(F_{fr,v}\right)$ is calculated by considering the lubricant as a Newtonian fluid, as shown in Equation (23) [52].

$$F_{fr,v,i} = \int_{a_i}^{b_i}\left(v\cdot\frac{\mu}{h} + \frac{h}{2}\cdot\frac{\partial p}{\partial x}\right)dx. \tag{23}$$

The dynamic viscosity of the lubricant (μ) is calculated by means of Equation (24) [53].

$$\mu = \mu_o\cdot e^{\left[ln\left(\frac{\mu_o}{\mu_\infty}\right)\cdot\left(1+\frac{p-p_{atm}}{c_p}\right)^z\left(\frac{T-138}{T_o-138}\right)^{-S_o}-1\right]} \tag{24}$$

where Z is the piezoelectric viscosity, S_o is the thermo-viscosity indices and μ_o is the dynamic viscosity of the lubricant under atmospheric conditions. The parameters Z and S_o are determined from Equations (25) and (26) [50].

$$Z = c_p\cdot\alpha_o\left[ln\left(\frac{\mu_0}{\mu_\infty}\right)\right]^{-1} \tag{25}$$

$$S_o = (T_o - 138)\cdot\beta_o\cdot\left[ln\left(\frac{\mu_0}{\mu_\infty}\right)\right]^{-1} \tag{26}$$

where β_o and α_o are thermo-viscosity coefficients and atmospheric piezo-viscosity. μ_∞ and c_p are constants defined via Equations (27) and (28).

$$\mu_\infty = 6.31\times 10^{-5}\ \text{Pa}\cdot\text{s} \tag{27}$$

$$c_p = 1.98\times 10^8\ \text{Pa}. \tag{28}$$

The asperity friction force $\left(F_{fr,s}\right)$ is determined by Equation (29).

$$F_{fr,s,i} = \int_{a_i}^{b_i} c_{fr}\cdot P_c\ dx \tag{29}$$

where c_{fr} is the metal-metal friction coefficient and P_c is the asperity contact pressure, which is determined by means of the Greenwood and Tripp model [54], as shown in Equation (30):

$$P_c = F_{5/2}(\lambda) \cdot \frac{16 \cdot \sqrt{2 \cdot \pi}}{15} \cdot \rho_s^2 \cdot \left(\sigma_c^2 + \sigma_p^2\right)^{5/4} r_c^{3/2} \cdot E \tag{30}$$

where r_c is the radius of curvature of asperities, ρ_s is the asperity density of the surface, E is the young's modulus between cylinder liner and ring. σ_c and σ_p are the surface roughness of the cylinder liner and piston ring.

The effective elastic modulus between the cylinder liner and ring ($E_{e,c}$), is calculated by the Equation (31).

$$\frac{1 - \vartheta_1^2}{E_1} + \frac{1 - \vartheta_2^2}{E_2} = \frac{2}{E_{e,c}} \tag{31}$$

where ϑ is the Poisson ratio, and E is the elastic modulus. Subscripts 1 and 2 represent the surface area of the cylinder liner and piston ring, respectively.

The term $F_{5/2}(\lambda)$ represents the Gaussian roughness distribution, which is calculated by Equation (32) [55].

$$F_{5/2}(\lambda) = \left\{ \begin{array}{c} -0.0046\lambda^5 + 0.057\lambda^4 - 0.296\lambda^3 + 0.785\lambda^2 - 1.078\lambda + 0.62, \ \lambda = \frac{h}{\sqrt{\sigma_p^2 + \sigma_r^2}} \leq 2.23 \\ 0, \ \lambda = \frac{h}{\sqrt{\sigma_p^2 + \sigma_r^2}} > 2.23 \end{array} \right\} . \tag{32}$$

Finally, the energy losses to friction in the piston are calculated by Equation (33).

$$E_{f,p} = \sum_{i=1}^{3} \left(\int_0^{2\pi} F_{fr,v,i} \cdot v \, d\theta + \int_0^{2\pi} F_{fr,s,i} \cdot v \, d\theta \right). \tag{33}$$

3.3. Energy Losses in Bearings

To describe the energy losses in the bearings, the mobility model is taken as a basis, which considers the trajectory inside the bearing, the location of the center of the journal, and the minimum thickness of the lubrication film [56]. Figure 2 describes the bearing geometry used for the model.
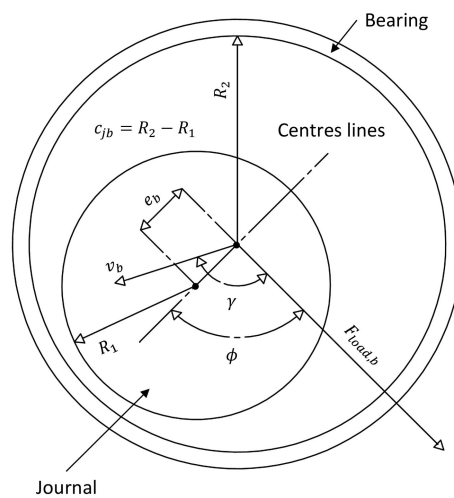

Figure 2. Bearing internal geometry.

The friction force applied to the bearings is determined from Equation (34) [56].

$$F_{fr,b} = \frac{2 \cdot v_b \cdot F_{load,b} \cdot \sin \gamma + \omega \cdot e_r \cdot c_{jb} \cdot F_{load,b} \cdot \sin \phi}{\omega \cdot D_b} + \frac{\mu \cdot \omega \cdot D_b^2 \cdot L_b \cdot J_1^{00}}{4 \cdot c_{jb}} \tag{34}$$

where μ is the dynamic oil viscosity, ω is the angular speed (this speed is considered to be the same for the bearing and journal), D_b is the bearing diameter, L_b is the bearing length, c_{jb} is the clearance between journal and bearing, v_b is the speed of the bearing centre displacement, ϕ is the angle between $F_{load,b}$ and the centre line and γ is the angle between $F_{load,b}$ and v_b. The eccentricity ratio (e_r) is calculated by Equation (35).

$$e_r = \frac{e_b}{c_{jb}} \tag{35}$$

where e_b is the eccentricity between the bearing centre and journal. $F_{load,b}$ is the instantaneous load applied to the bearing, and its value depends on the location (i.e., crankshaft or connecting rod). The applied load on the connecting rod bearing (bearing 1) is determined directly from the dynamic analysis of the piston mechanism. In the case of crankshaft bearings (bearing 2 and bearing 3), the load they support is considered to be half the force exerted on bearing 1. This consideration is in accordance with the results recorded in the literature [57]. Figure 3 shows the forces applied to the previously described bearings.
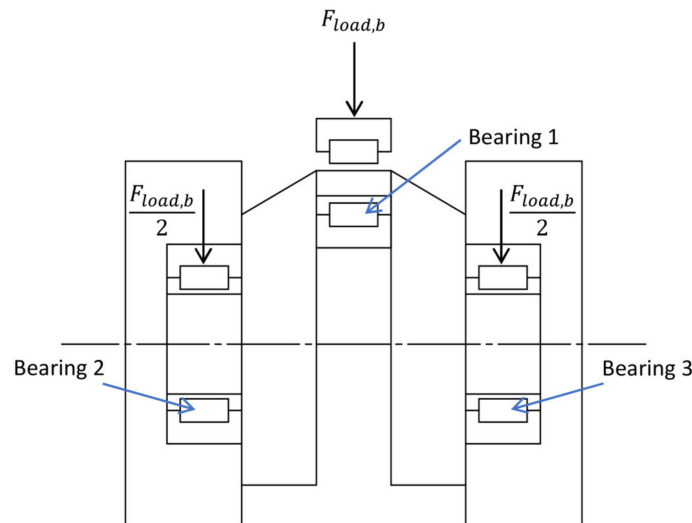

Figure 3. Load diagram for engine bearings.

The thickness of the lubrication film on the bearings is determined by Equation (36).

$$h = c_{rc} \cdot \left(1 - c_{jb} \cdot \cos \phi\right). \tag{36}$$

where c_{rc} is the radial clearance in the bearings.

The parameter J_1^{00} present in Equation (34) describes the behavior of the extension and the change in thickness of the lubrication film around the bearing. To calculate this parameter, the equation proposed by Taylor is used [56], which is shown in Equation (37).

$$J_1^{00} = \int_0^{2\pi} \frac{d\theta}{e_r \cdot \cos \theta + 1} = \frac{2\pi}{\sqrt{1 - e_r^2}}. \tag{37}$$

The model used in the present work is considered a quasi-stable condition, which implies that there is no translational movement in the bearing. Therefore, the speed of the displacement of the bearing center is zero ($v_b = 0$) [26]. Hence, Equation (34) can be expressed, as shown in Equation (38) [56]:

$$F_{fr,b} = \frac{e_r \cdot c_{jb} \cdot F_{load,b} \cdot \sin\phi}{D_b} + \frac{\mu \cdot \omega \cdot D_b^2 \cdot \pi \cdot L_b}{2 \cdot c_{jb} \sqrt{1 - e_r^2}}. \tag{38}$$

The angle between $F_{load,b}$ and the centre line (ϕ), is determined from Equation (39).

$$\phi = \tan^{-1}\left(\frac{\pi}{4} \cdot \sqrt{\frac{1 - e_r^2}{e_r^2}} \right). \tag{39}$$

Solving Equations (35), (38) and (39) together determine the energy losses by the friction process in the bearings, which is calculated by Equation (40).

$$E_{f,b} = \sum_{i=1}^{n=i} \int_0^{2\pi} \frac{D_{b,i} \omega \cdot F_{fr,b,i}}{2} d\theta \tag{40}$$

where n is the total number of bearings to consider.

4. Numerical Methodology

The methodology used in this research is divided into two parts, which consist of an experimental part for the compilation of test data that allows determining the energy losses mentioned in Section 2 and a numerical part for the solution of the equations shown in Section 3. The experimental test bench and the measuring instruments used for the study are described in Section 5.

The equations described in Section 3 are solved using the solver tool ode45 of the Matlab® software. Figure 4 describes the diagram for the development of the experimental and numerical methodology.
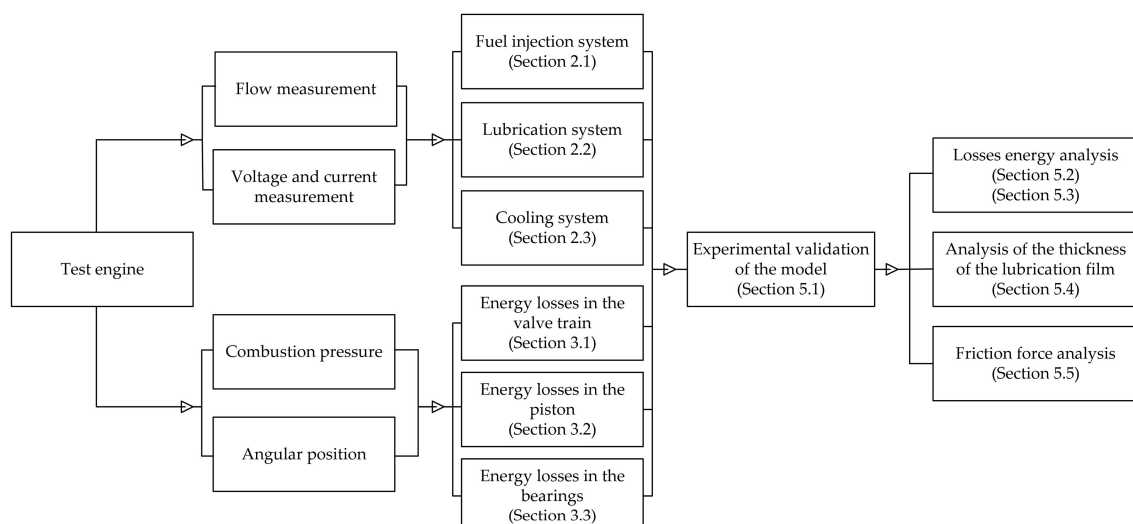

Figure 4. Methodology used in this study.

Based on the characteristics of the engine and the operating conditions, the losses energy calculations caused by the auxiliary systems (Section 2) and the friction processes (Section 3) are made. Verification of the model results is carried out through experimental validation, which is discussed in Section 6.1. Finally, the results of the model are used to evaluate the contribution of the energy losses

of each system and process, the influence of the engine operating conditions, and the analysis of the lubrication film on the components.

5. Experimental Methodology

The experimental tests were carried out on a test bench made up of a single-cylinder diesel engine. The technical characteristics of the engine are shown in Table 1.

Table 1. Single cylinder diesel engine.

Engine	SOKAN
Model	SK-MDF300
Compression ratio	20:1
Number of cylinders	1
Fuel injection system	Direct injection
Cylinder stroke/bore [mm]	63/78
Intake system	Naturally Aspirated
Volume [cc]	300
Cycle	4 Strokes

The properties of the lubricant used are shown in Table 2. In the case of fuel, commercial diesel was used with an addition of 0.075 LPM of hydrogen, which entered through the air intake system of the engine. The properties of diesel and hydrogen are described in Table 3.

Table 2. Properties of the engine lubricant.

SAE15W-40	
Density at 20 °C	0.864 g/cm^3 (DIN 51757)
Pourpoint	−33 °C (ISO 3016)
Viscosity at 40 °C	91.76 mm^2/s
Flashpoint	224 °C (DIN ISO 2592)
Lower explosion limit	0.6 vol%
Upper explosion limit	6.5 vol%

Table 3. Diesel and hydrogen properties.

| Properties	Units	Diesel	Hydroxy Gas
Density	kg/m^3	0.827	0.084
Kinematic viscosity	cSt	3.2	-
Flash point	°C	74	-
Calorific value	MJ/kg	41	115

For the analysis of the energy losses of the engine, nine operating modes were established, as shown in Figure 5. These modes consist of variations in torque and rotation speed between 4–6 Nm and 3400–3800 rpm, respectively. In this way, it is possible to evaluate the energy losses that occur in the engine for low, medium, and high load conditions, thus covering the different conditions in which the engine can operate.

The control of the torque and rotation speed is carried out by means of a dynamometer, which is coupled to the engine shaft. To calculate the energy losses in the fuel injection system, a gravimetric meter is used to determine the fuel flow (OHAUS PA313, OHAUS Corporation, Parsippany, NJ, USA). Additionally, the common rail pressure measurement is performed by means of a pressure sensor (KISTLER Type 4067-E, KISTLER, Winterthur, Switzerland). The measurement of the lubrication flow is carried out by using a turbine-type flow sensor, which is used to calculate the losses in the lubrication system. Finally, the electrical characteristics of voltage and current of the fan in charge of

cooling the engine are recorded. For this, a digital multimeter (Fluke 15b-F15b, Fluke Corporation, Everett, WA, USA) is used. The engine test bench diagram is shown in Figure 6.
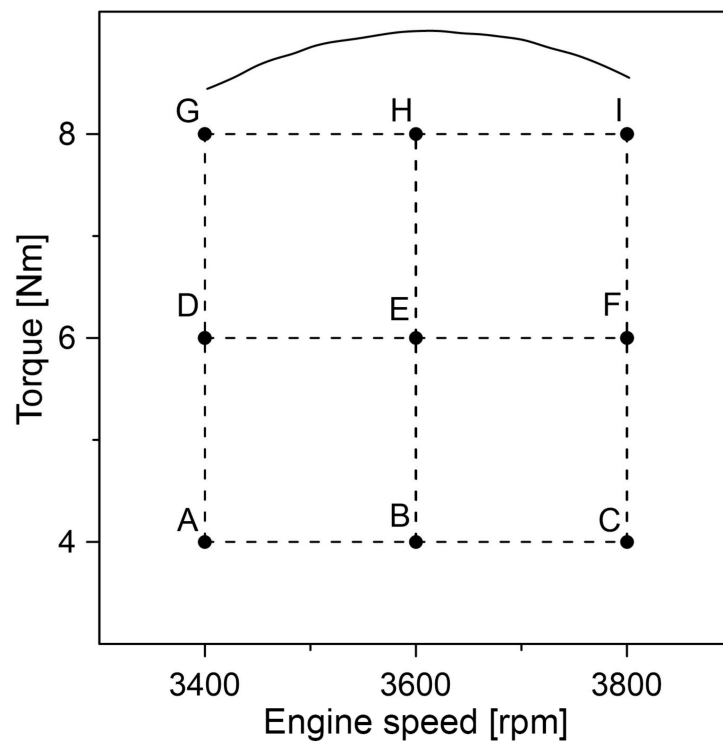
Figure 5. Engine operating modes, A: 4 Nm-3400 rpm, B: 4 Nm-3600 rpm, C: 4 Nm-3800 rpm, D: 6 Nm-3400 rpm, E: 4 Nm-3600 rpm, F: 6 Nm-3800 rpm, G: 8 Nm-3400 rpm, H: 8 Nm-3600 rpm, I: 8 Nm-3800 rpm.
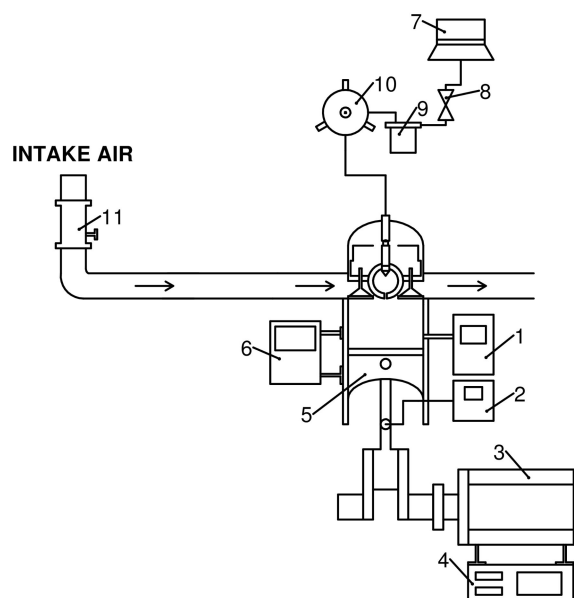
Figure 6. Engine test bench. 1. Data acquisition (DAQ), 2. Crank angle encoder, 3. Dynamometer, 4. Resistive bench, 5. Engine, 6. Median variables DAQ, 7. Diesel tank, 8. Fuel inlet valve, 9. Fuel filter, 10. Injection pump, 11. Airflow meter.

To calculate the energy losses for friction processes, it is necessary to determine the piston's position and the pressure in the combustion chamber since they are input data for the solution of the equations proposed. The combustion pressure measurement is carried out utilizing a piezoelectric sensor (KISTLER type 7063-A, KISTLER, Winterthur, Switzerland) installed inside the chamber. Synchronization between chamber pressure and the crankshaft rotation angle is done using an angle encoder (BECK ARNLEY 180-0420, Beck / Arnley Company, Smyrna, TN, USA). Table 4 shows the characteristics of the measurement instruments used.

Table 4. Measurement instruments.

Parameter	Instrument	Manufacturer	Range	Accuracy
Angle	Crankshaft angle	Beck Arnley 180-0420	5–9999 RPM	0.03%
Cylinder pressure	Piezoelectric transducer	KISTLER type 7063-A	0–250 bar	< ±0.5%
Airflow	Air mass sensor	BOSCH OE-22680 7J600	0–125 g/s	1%
Fuel measuring	Gravimetric meter	OHAUS-PA313	0–310 g	1.5%
Temperature	Temperature sensor	Type K	−200–1370 °C	0.1%
Pressure	Pressure sensor	KISTLER Type 4067-E	0–200 bar	1%

6. Results and Discussions

6.1. Experimental Validation

To verify the prediction capacity of the models proposed in Sections 2 and 3, the total energy losses caused by engine friction in the different operating modes are experimentally determined. The evaluation of friction losses is determined by calculating the indicated mean effective pressure (IMEP) and brake mean effective pressure (BMEP), as shown in Equation (41).

$$FMEP = IMEP - BMEP \tag{41}$$

where FMEP (Friction Mean Effective Pressure) represents the power required to overcome engine friction. Equation (41) can be rewritten as:

$$FMEP = \frac{\oint pdV}{v_d} - \frac{4 \cdot \pi \cdot T}{v_d} \tag{42}$$

where T is the measured torque of the engine and v_d is the displaced volume in the chamber.

In the case of auxiliary systems, the characteristic curve of the fuel and lubricant pumps supplied by the manufacturer is used to determine the power consumption associated with each quantity of flow. For the cooling system, the power consumed is calculated directly by the current and voltage conditions of the engine fan. Figure 7 shows the comparison between the results of the model and the experimental ones.

Figure 7 shows that the proposed model maintains the same trend when compared with the experimental results. An average error of 6% was obtained between the model estimates and the experimental data.

In general, low and medium load conditions have the lowest error rates. As higher rotational speeds and torques are operated, the error in the model estimates tends to increase. The foregoing can be the consequence of greater operational instability of the engine under high load conditions, which can be attributed to variations in chamber pressure throughout the combustion cycle, greater vibrations, and changes in the characteristics of the lubricant. However, the maximum error recorded is less than 10%.

In the following sections (Sections 6.2–6.5), the analysis of the calculations obtained from the auxiliary systems and the friction processes in the engine is performed.
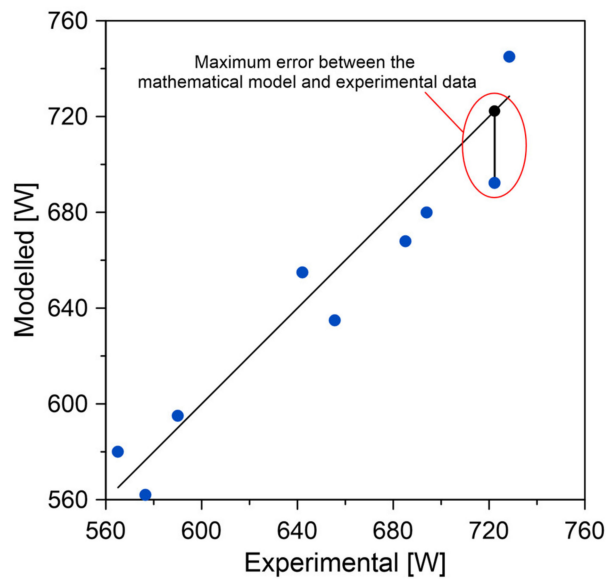
Figure 7. Energy losses by auxiliary systems and friction processes were obtained experimentally and modeled.

6.2. Analysis of Energy Losses in the Engine

Figure 8 shows the energy losses of the auxiliary engine systems for the different operating conditions. Notice that the bar graph shown in Figure 8 displays the contribution of each system represented with different patterns as a portion of the total energy losses.
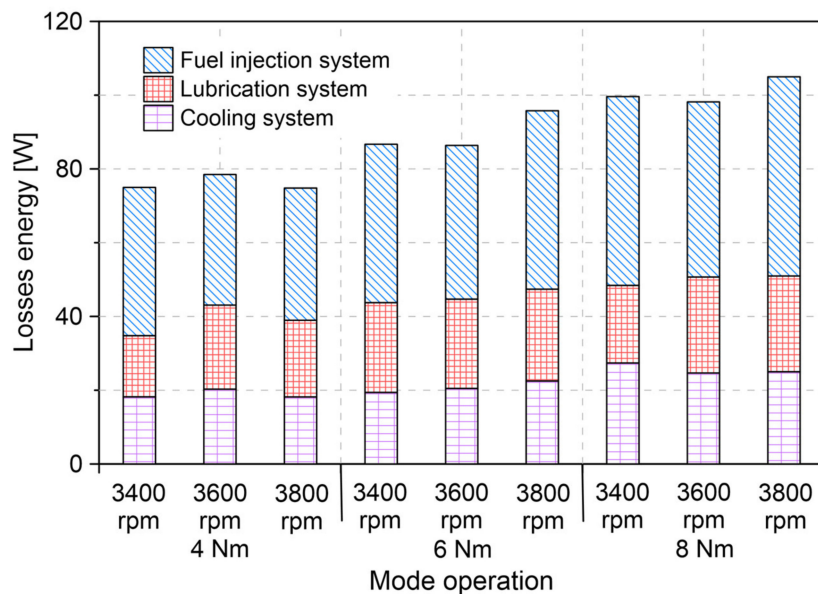
Figure 8. Energy losses in auxiliary systems.

According to the results, the greatest energy losses occur in the fuel injection system. On average, an energy loss of 22.9, 21.8, and 44.1 W was observed for the lubrication, cooling, and fuel injection systems, respectively. The maximum values of energy losses in each of the above systems are 26 W, 27.4 W, and 54 W, which is equivalent to 0.40, 0.39, and 0.73% of the chemical energy of the fuel injected into the engine.

For the fuel injection system, it was observed that the energy loss tends to increase with the increase in the rotational speed and mechanical power of the engine. The foregoing is a consequence

of the greater need for fuel pumping to reach the highest levels of load and engine speed. In the range of test conditions, the energy loss was of the fuel system varies between 35–54 W.

In the case of the cooling system, it is shown that the pumping power is increased mainly by the increase in torque in the engine. In general, increases in rotation speed do not cause a considerable change in the consumption of the cooling pump. However, by increasing the torque of the engine by 2 Nm, the energy consumed increases by 24%. The energy consumed by the lubrication system is considerably increased for rotational speeds above 3600 rpm. This is a consequence of the greater need for lubrication flow for components subjected to high accelerations. For the test conditions, the consumption of the lubrication pump was observed between 17–26 W, which is similar to the energy loss developed by the cooling pump.

Figure 9 shows the energy losses produced by the friction processes in the bearings, valve train, and piston.
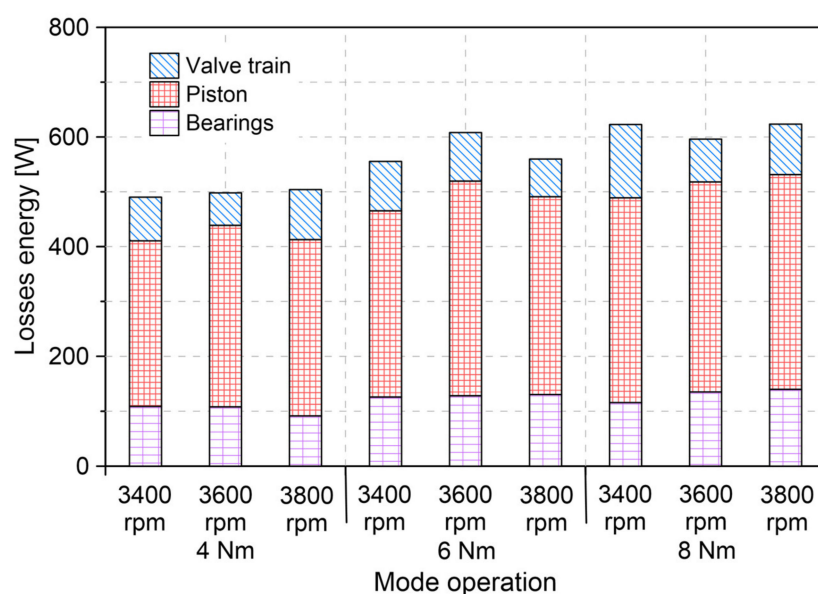

Figure 9. Losses of energy by friction.

The results indicate that the main friction energy loss occurs in the piston. In general, the energy loss to friction in the piston is three to four times greater than in the bearings and valve train. On average, a loss of 120.4, 86.8, and 354.72 W was observed for the bearings, valve train, and piston, which is equivalent to 1.85, 1.34, and 5.47% of the total energy available from fuel injection.

In addition, it can be observed that the energy loss in the piston increases with the torque and the rotational speed of the engine. This can be a consequence of the friction coefficient, which is directly related to the speed of the bodies. For the energy loss in the valve train and the bearings, it is noticed that the greatest losses occur at the highest torque. In contrast, the increase in the rotation speed does not produce a significant change in the increase in friction losses.

6.3. Analysis of Energy Loss Distributions

Figure 10 shows the average distribution of the total energy losses of the engine due to friction processes and auxiliary systems.

The results show that friction processes are the main contributors to engine energy losses. Among this type, the piston occupies more than half of the total losses (55%), followed by the bearings (19%) and the valve train (13%). In the case of auxiliary systems, it was found that the lubrication and cooling systems present a similar share of energy loss, which corresponds to between 3% and 4%, respectively. Of the auxiliary systems, fuel injection is the one with the highest percentage of total losses, reaching approximately 6.6%.
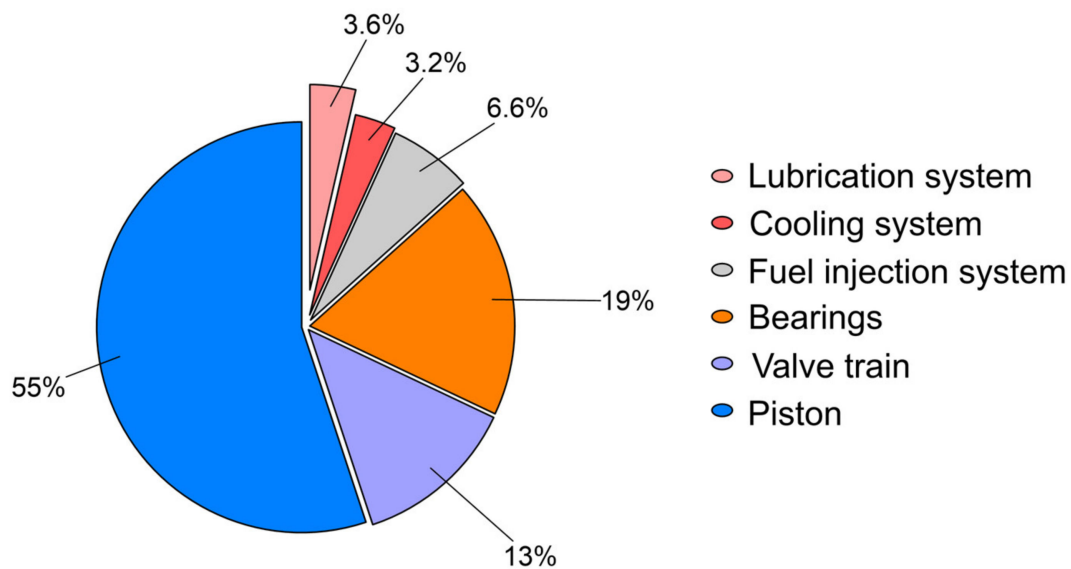
Figure 10. Distribution of energy losses.

6.4. Lubrication Film Analysis

6.4.1. Piston

In Figure 11, the minimum thickness of the lubrication film between the piston skirt and the cylinder liner is shown.
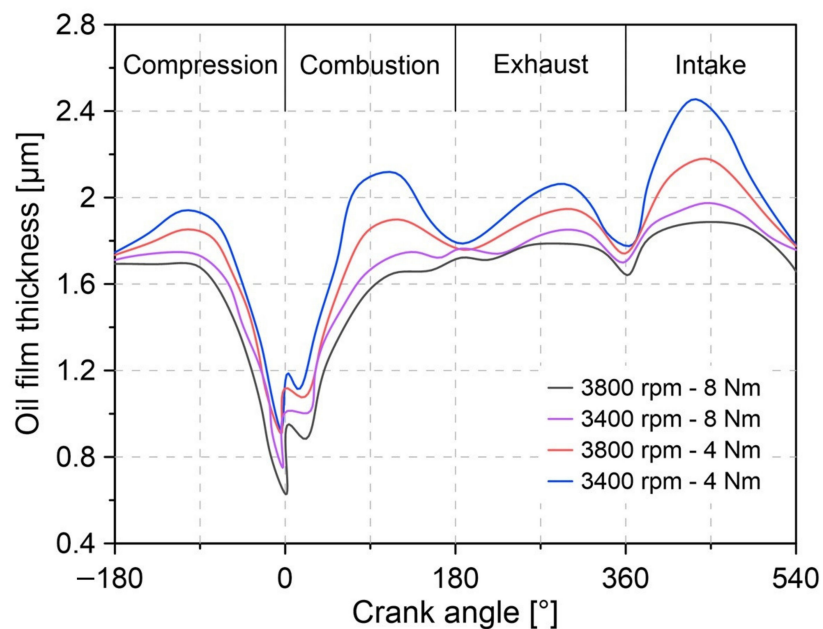

Figure 11. Minimum thickness of the lubrication film on the piston.

The results show that the thickness of the lubrication film decreases with increasing rotational speed and engine torque. Increasing these parameters causes an increase in the temperature of the lubricant, which reduces the viscosity of the oil. The foregoing allows explaining the reduction in the lubrication film. The thickness of the lubrication film is recorded during the compression and combustion stage, which can be an effect of the increase in pressure in the piston rings.

The minimum lubrication thickness recorded for the operating conditions corresponds to 0.63 μm. Specifically, an increase of 400 rpm in the rotational speed of the engine causes a reduction of the thickness by 11%, while an increase of 4 Nm in torque reduces approximately 25%.

6.4.2. Valve Train

The valve train is composed of different elements such as bearings, valve stem, and camshaft. These elements are subjected to friction, which leads to energy losses. However, the contact between the follower and the cam represents the largest contribution to the energy losses of the valve train system. Figure 12 shows the energy loss produced by the follower-cam contact throughout the combustion cycle.
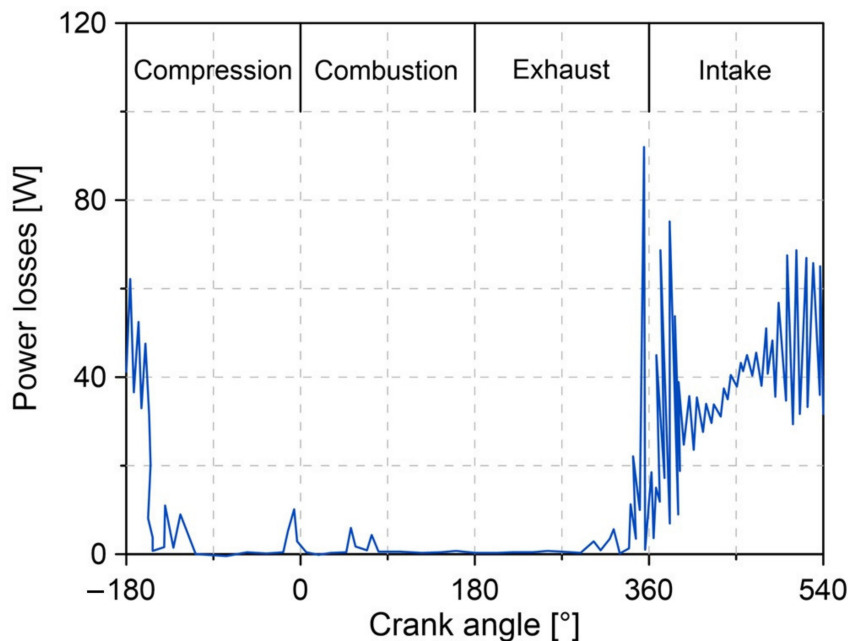
**Figure 12.** Power losses in valve train (3800 rpm–8 Nm).

The results in Figure 12 indicate that the intake stage is where the energy losses of the valve train are concentrated. This can be explained by considering that in this location, the lobe of the cam exerts high pressure on the roller, which is necessary to force the movement of the valve. Therefore, the friction force reaches its maximum value in this condition. This conclusion can be validated by observing the thickness of the lubrication film between the follower and the cam, as shown in Figure 13. Here, the thickness remains relatively constant with a value of 2 μm during the compression stage, combustion, and escape. However, during the intake stage, the thickness of the film decreases until it reaches a minimum value of 0.10 μm.
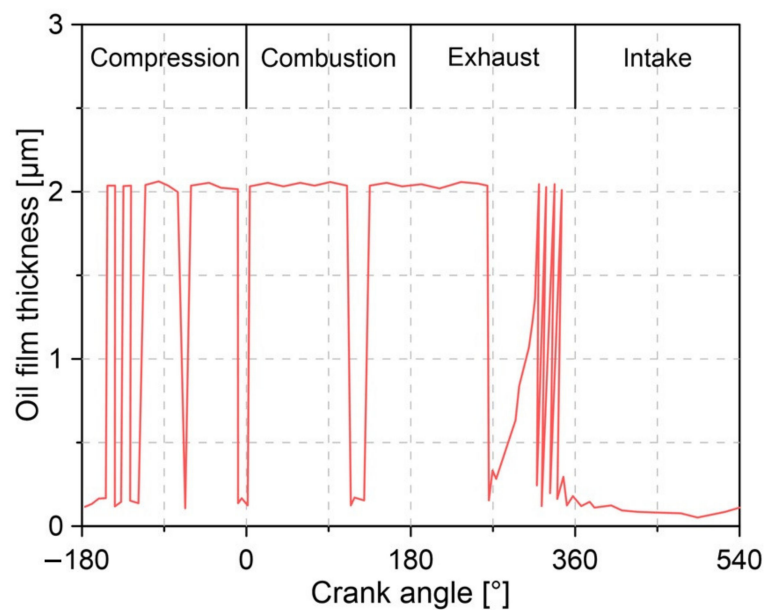
Figure 13. Minimum thickness of the lubrication film between follower-cam (3800 rpm–8 Nm).

6.4.3. Bearings

Figure 14 shows the minimum lubrication film thickness for bearings 1, 2, and 3 (see Figure 3).
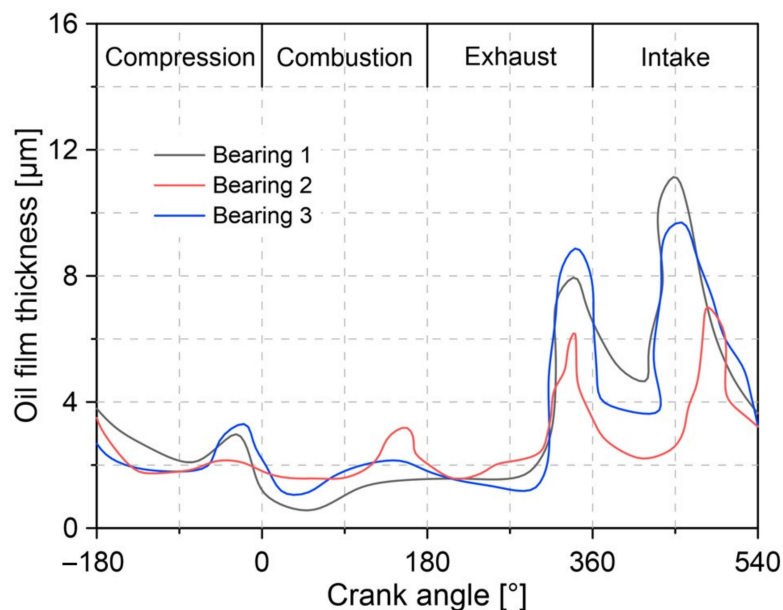
Figure 14. Minimum lubrication film thickness for engine bearings (3800 rpm–8 Nm).

The big end bearing of the connecting rod (bearing 1) is in charge of supporting the highest load conditions because the pressures resulting from the combustion cylinder are directly applied in this location. Bearings 2 and 3 handle a lesser load. This behavior can be seen when comparing the minimum thicknesses of the lubrication film achieved by the three bearings. For an operating condition of 3800 rpm–8 Nm in the engine, it was observed that the minimum thickness in the lubrication film is 0.57, 1.56, and 1.13 μm for bearing 1, 2, and 3, respectively. The lower thickness located in bearing 1 is an indication that it is subjected to a greater load.

The lower thicknesses of the lubrication film for all the bearings are obtained during the compression and combustion stage, which is an effect of the high pressures in the combustion chamber

developed in these stages. The results indicate that the thickness of bearings 1, 2, and 3 is reduced by 10.57, 5.43, and 8.57 µm, respectively, throughout the combustion cycle.

6.5. Friction Force Analysis

Figure 15 shows the change in the friction force on the piston during the combustion cycle.
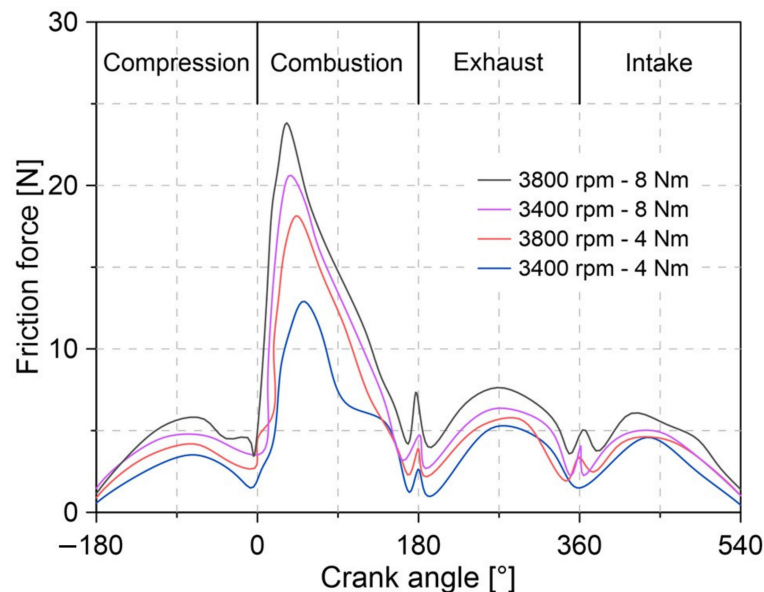

Figure 15. Variation of friction force on piston rings.

The results show that the maximum levels of friction force occur at the top dead center and during the combustion stage. This can be the consequence of a mixed lubrication condition, in which there is greater interaction between the surface thickness of the rings and the cylinder liner. For the operational condition with maximum torque (8 Nm) and rotational speed (3800 rpm), the highest value of friction force (23.82 N) was obtained.

In general, the friction force is lower during the intake and exhaust stages. This can be attributed to the reduction of friction interactions due to the low combustion pressures during these stages. This behavior is in accordance with the predictions reported in the literature [58].

Figure 16 shows the friction force in the valve train for the different operating conditions.

The results show that the friction force in the valve train varies between 1.91 N and 3.62 N for the tested operating conditions. On average, increasing the rotational speed by 200 rpm and the torque by 2 Nm enlarge the friction force by 9% and 26%, respectively. This is associated with the beginning of a mixed lubrication regime between the follower and cam.

Figure 17 shows the friction force acting on the main bearing of the crankshaft (bearing 1).

The results of Figure 17 show a behavior similar to that described in Figure 16. It was observed that the friction force has a strong influence on the rotation speed and the torque of the engine. For the operating conditions tested, the friction force is maintained in a range of 1.07 N to 4.81 N.
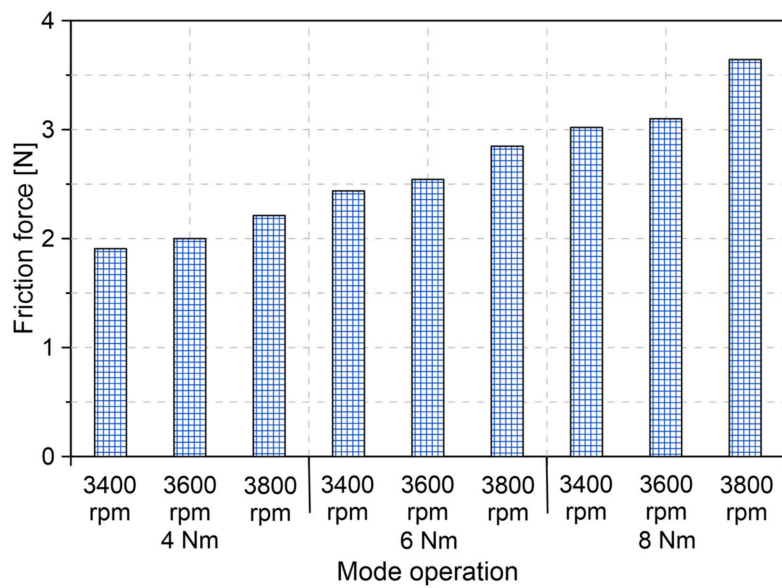
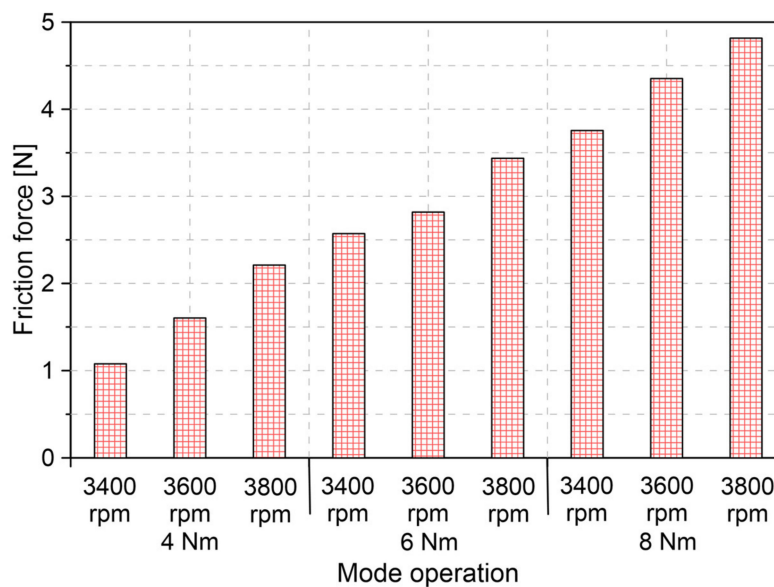**Figure 16.** Friction forces in the valve train.

Figure 17. Friction forces in the main bearing of the crankshaft.

7. Conclusions

In this research, a numerical methodology is developed for estimating the combined effects of energy losses in the auxiliary systems (fuel injection system, lubrication system, and cooling system) and the friction processes of the engine components (piston, valve train, and bearings). The methodology incorporated mathematical models in which the dynamic characteristics and tribological conditions present in the piston, valve train, and bearings are considered. Also, the model is capable of determining the consumption of fuel, lubrication, and cooling pumps, as well as the lubrication film conditions on the piston, valve train, and bearings.

The analysis of the auxiliary systems demonstrated that the fuel injection system features the greatest energy losses. Indeed, these losses double those obtained in the lubrication and cooling systems. In the case of the latter two, it was observed that both systems present an average consumption of 22.35 W for the tested conditions (4–8 Nm and 3400–3800 rpm). The energy losses of the fuel injection

system, lubrication, and coolant are equal to 0.61, 0.30, and 0.31% of the total chemical energy of the injected fuel, respectively.

For energy losses due to friction processes, it was observed that the main losses are located in the piston, which reaches a maximum value of 391 W. In the case of the valve train and the bearings, energy losses were found between 59–140 W for the operating range. On average, the energy losses by friction processes in the piston, valve train, and bearings represent 5.47, 1.34, and 1.85% of the total fuel energy, respectively.

In general, friction processes cover 87% of total mechanical losses, of which 55% is produced by the interaction of the pistons. The fuel injection system represents 6.5% of total mechanical losses.

The analysis of the lubrication film in the piston showed a decreasing trend as the torque and engine rotation speed increase, reaching a minimum thickness of 0.63 µm in the highest load condition. For the valve train, it is shown that its energy loss occurs mainly during the inlet and exhaust stage, in which the minimum lubrication film thickness is 0.10 µm. By analyzing the three crankshaft bearings, it was shown that the connecting rod bearing is subjected to a higher load, which causes a reduction in the thickness of the lubrication film.

In general, the model developed in this work demonstrated to be a useful tool to estimate the energy losses produced in the auxiliary systems and the components subjected to friction. This can be applied to different operating conditions, including the type of fuel and geometric characteristics of a specific engine. Therefore, the numerical methodology implemented helps to analyze the influence of modifications and/or design of engine components on the global behavior of energy losses, which contributes to identifying critical lubrication conditions that minimize the energy wasted in internal combustion engines.

Abbreviations

The following abbreviations are used in this manuscript:

E	Energy losses
$\dot{V}$	Volumetric flow of fuel
P_{cr}	Common rail pressure
$\dot{m}$	Mass flow
ΔP	Pressure drop
D	Diameter
L	Length
f	Friction factor
g	Gravity
r	Roughness
N	Rotational speed

k	Fan factor
V_s	Supply voltage
I	Electric current
$F_{cf,v}$	Contact friction between the follower and the cam
$F_{ac,v}$	Asperity contact force between the follower and the cam
$F_{vf,v}$	Viscous friction force between the follower and the cam
c_p	Coefficient of the shear strength
l_c	Load carried by the asperities
A_a	Asperity area
τ_{ss}	Eyring shear stress
r_s	Composite surface roughness parameter
r_a	Asperities radius of curvature
ρ_a	Asperity density
E_e	Effective elastic modulus
H_c	Hertzian contact area
r_e	Equivalent radius of curvature
w_{cam}	Cam width
$F_{n,v}$	Force normal
ϑ_{foll}	Poisson ratio of the follower
ϑ_{cam}	Poisson ratio of the cam
E_{foll}	Young module of the follower and cam
E_{cam}	Young module of the cam
F_2	Statistical function
s_p	Separation parameter
h	Thickness of the lubrication film
c_{pv}	Pressure viscosity coefficient
r_{cc}	Combined radius of curvature
v_e	Entrainment velocity
v_c	Contact velocity
n_{ind}	Number of intake valves
n_{exh}	Number of exhaust valves
v	Piston velocity
p	Lubrication film pressure
$F_{fr,p}$	Frictional force produced between the ring face and the cylinder liner
$F_{fr,s}$	Asperity friction force between the ring face and the cylinder liner
$F_{fr,v}$	Viscous friction force between the ring face and the cylinder liner
Z	Piezoelectric viscosity
S_o	Thermo-viscosity indice
β_o	Thermo-viscosity coefficients
α_o	Atmospheric piezo-viscosity
c_{fr}	Metal-metal friction coefficient
P_c	Asperity contact pressure
r_c	Radius of curvature of asperities
ρ_s	Asperity density of the surface
σ_c	Surface roughness of the cylinder liner
σ_p	Surface roughness of the piston ring
$F_{5/2}$	Gaussian roughness distribution
ω	Angular speed
D_b	Bearing length
L_b	Bearing length
c_{jb}	Clearance between journal and bearing
v_b	Speed of the bearing centre displacement
e_r	Eccentricity ratio
e_b	Eccentricity between the bearing centre and journal
$F_{load,b}$	Instantaneous load applied to the bearing
c_{rc}	Radial clearance

Greek Letters

η	Efficiency
μ	Dynamic viscosity
ρ	Density

Subscripts

f	Fuel injection system
lub	Oil pump
o	Atmospheric conditions
c	Cooling system

References

1. Zhang, Q.; Chen, G.; Zheng, Z.; Liu, H.; Xu, J.; Yao, M. Combustion and emissions of 2,5-dimethylfuran addition on a diesel engine with low temperature combustion. *Fuel* **2013**, *103*, 730–735. [CrossRef]
2. Xiao, H.; Guo, F.; Li, S.; Wang, R.; Yang, X. Combustion performance and emission characteristics of a diesel engine burning biodiesel blended with n-butanol. *Fuel* **2019**, *258*, 115887. [CrossRef]
3. Aydin, H.; Ilkılıç, C. Effect of ethanol blending with biodiesel on engine performance and exhaust emissions in a CI engine. *Appl. Therm. Eng.* **2010**, *30*, 1199–1204. [CrossRef]
4. Xiao, H.; Guo, F.; Wang, R.; Yang, X.; Li, S.; Xiao, H. Combustion performance and emission characteristics of diesel engine fueled with iso-butanol/biodiesel blends. *Fuel* **2020**, *268*, 117387. [CrossRef]
5. Erdoğan, S.; Balki, M.K.; Aydın, S.; Sayın, C. Performance, emission and combustion characteristic assessment of biodiesels derived from beef bone marrow in a diesel generator. *Energy* **2020**, *207*, 118300. [CrossRef]
6. Mejía, A.; Leiva, M.; Rincón-Montenegro, A.; Gonzalez-Quiroga, A.; Duarte, J. Experimental assessment of emissions maps of a single-cylinder compression ignition engine powered by diesel and palm oil biodiesel-diesel fuel blends. *Case Stud. Therm. Eng.* **2020**, *19*, 100613. [CrossRef]
7. Ochoa, G.V.; Acevedo, C.; Duarte, J. Thermo-Economic Assessment of a Gas Microturbine-Absorption Chiller Trigeneration System under Different Compressor Inlet Air Temperatures. *Energies* **2019**, *12*, 4643. [CrossRef]
8. Singh, D.; Sharma, D.; Soni, S.; Inda, C.S.; Sharma, S.; Sharma, P.K.; Jhalani, A. A comprehensive review of physicochemical properties, production process, performance and emissions characteristics of 2nd generation biodiesel feedstock: Jatropha curcas. *Fuel* **2021**, *285*, 119110. [CrossRef]
9. European Commission. Setting emisison performace standards for new passenger cars as part of the community's integrated approach to reduce CO_2 emissions from light-duty vehicles. *Off. J. Eur. Commun.* **2009**, *140*, 5–6.
10. Duarte, J.; Garcia, J.; Jimenez, J.; Sanjuan, M.E.; Bula, A.; Gonzalez, J. Auto-ignition control in spark-ignition engines using internal model control structure. *J. Energy Res. Technol.* **2017**, *139*, 022201. [CrossRef]
11. Pietikäinen, M.; Väliheikki, A.; Oravisjärvi, K.; Kolli, T.; Huuhtanen, M.; Niemi, S.; Virtanen, S.; Karhu, T.; Keiski, R.L. Particle and NOx emissions of a non-road diesel engine with an SCR unit: The effect of fuel. *Renew. Energy* **2015**, *77*, 377–385. [CrossRef]
12. Beatrice, C.; Di Iorio, S.; Guido, C.; Napolitano, P. Detailed characterization of particulate emissions of an automotive catalyzed DPF using actual regeneration strategies. *Exp. Therm. Fluid Sci.* **2012**, *39*, 45–53. [CrossRef]
13. Diaz, G.A.; Duarte, J.; Rincon, A.; Fontalvo, A.; Bula, A.; Padilla, R.V.; Orozco, W. Characteristics of Auto-Ignition in Internal Combustion Engines Operated With Gaseous Fuels of Variable Methane Number. *J. Energy Resour. Technol.* **2017**, *139*, 042205. [CrossRef]
14. Diaz, G.A.; Duarte, J.; Garcia, J.; Rincon, A.; Fontalvo, A.; Bula, A.; Padilla, R.V. Maximum Power From Fluid Flow by Applying the First and Second Laws of Thermodynamics. *J. Energy Resour. Technol.* **2017**, *139*, 032903. [CrossRef]
15. Ochoa, G.V.; Isaza-Roldan, C.; Duarte, J. Economic and Exergo-Advance Analysis of a Waste Heat Recovery System Based on Regenerative Organic Rankine Cycle under Organic Fluids with Low Global Warming Potential. *Energies* **2020**, *13*, 1317. [CrossRef]
16. Forero, J.D.; Ochoa, G.V.; Alvarado, W.P. Study of the Piston Secondary Movement on the Tribological Performance of a Single Cylinder Low-Displacement Diesel Engine. *Lubricants* **2020**, *8*, 97. [CrossRef]

17. Duarte Forero, J.; Valencia Ochoa, G.; Piero Rojas, J. Effect of the Geometric Profile of Top Ring on the Tribological Characteristics of a Low-Displacement Diesel Engine. *Lubricants* **2020**, *8*, 83. [CrossRef]

18. Knauder, C.; Allmaier, H.; Sander, D.E.; Salhofer, S.; Reich, F.M.; Sams, T. Analysis of the Journal Bearing Friction Losses in a Heavy-Duty Diesel Engine. *Lubricants* **2015**, *3*, 142–154. [CrossRef]

19. Morawitz, U.; Mehring, J.; Schramm, L. Benefits of Thermal Spray Coatings in Internal Combustion Engines, with Specific View on Friction Reduction and Thermal Management. *SAE Tech. Pap. Ser.* **2013**. [CrossRef]

20. Tormos, B.; Ramírez, L.; Johansson, J.; Björling, M.; Larsson, R. Fuel consumption and friction benefits of low viscosity engine oils for heavy duty applications. *Tribol. Int.* **2017**, *110*, 23–34. [CrossRef]

21. Tomanik, E. Friction and wear bench tests of different engine liner surface finishes. *Tribol. Int.* **2008**, *41*, 1032–1038. [CrossRef]

22. Consuegra, F.; Bula, A.; Guillín, W.; Sánchez, J.; Duarte, J. Instantaneous in-Cylinder Volume Considering Deformation and Clearance due to Lubricating Film in Reciprocating Internal Combustion Engines. *Energies* **2019**, *12*, 1437. [CrossRef]

23. Hoshi, M. Reducing friction losses in automobile engines. *Tribol. Int.* **1984**, *17*, 185–189. [CrossRef]

24. Dowson, D.; Taylor, C.M.; Yang, L. Friction modelling for internal combustion engines. In *Tribology Series*; Elsevier: Amsterdam, The Netherlands, 1996; pp. 301–318.

25. DuBois, G.B.; Ocvirk, F.W. Analytical Derivation and Experimental Evaluation of Short-Bearing Approximation for Full Journal Bearings. *Natl. Advis. Comm. Aeronaut.* **1953**, *1157*, 1–32.

26. Taraza, D.; A Henein, N.; Bryzik, W. *Friction Losses in Multi-Cylinder Diesel Engines*; SAE International: Warrendale, PA, USA, 2000.

27. Furuhama, S.; Sasaki, S. Effect of oil properties on piston frictional forces. *Int. J. Veh. Des.* **1986**. [CrossRef]

28. Tian, T. Dynamic behaviours of piston rings and their practical impact. Part 2: Oil transport, friction and wear of ring/liner interface and the effects of piston and ring dynamics. *Proc. Inst. Mech. Eng. Part J: J. Eng. Tribol.* **2002**, *216*, 229–248. [CrossRef]

29. Liu, C.; Lu, Y.; Zhang, Y.-F.; Li, S.; Müller, N. Numerical study on the lubrication performance of compression ring-cylinder liner system with spherical dimples. *PLoS ONE* **2017**, *12*, e0181574. [CrossRef]

30. Avan, E.Y.; Spencer, A.; Dwyer-Joyce, R.S.; Almqvist, A.; Larsson, R. Experimental and numerical investigations of oil film formation and friction in a piston ring–liner contact. *Proc. Inst. Mech. Eng. Part J J. Eng. Tribol.* **2012**, *227*, 126–140. [CrossRef]

31. Jocsak, J.; Wong, V.W.; Tian, T. The Effects of Cylinder Liner Finish on Piston Ring-Pack Friction. In Proceedings of the ASME 2004 Internal Combustion Engine Division Fall Technical Conference, Long Beach, CA, USA, 24–27 October 2004; pp. 841–849. [CrossRef]

32. Allmaier, H.; Sander, D.E.; Reich, F. Simulating Friction Power Losses in Automotive Journal Bearings. *Procedia Eng.* **2013**, *68*, 49–55. [CrossRef]

33. Sander, D.; Allmaier, H.; Priebsch, H.; Reich, F.; Witt, M.; Füllenbach, T.; Skiadas, A.; Brouwer, L.; Schwarze, H. Impact of high pressure and shear thinning on journal bearing friction. *Tribol. Int.* **2015**, *81*, 29–37. [CrossRef]

34. Turturro, A.; Rahmani, R.K.; Rahnejat, H.; Delprete, C.; Magro, L. Assessment of Friction for Cam-Roller Follower Valve Train System Subjected to Mixed Non-Newtonian Regime of Lubrication. In *ASME 2012 Internal Combustion Engine Division Spring Technical Conference*; ASME International: New York, NY, USA, 2012; pp. 917–923.

35. Masjedi, M.; Khonsari, M. Film Thickness and Asperity Load Formulas for Line-Contact Elastohydrodynamic Lubrication With Provision for Surface Roughness. *J. Tribol.* **2012**, *134*, 011503. [CrossRef]

36. Priest, M.; Taylor, C. Automobile engine tribology—Approaching the surface. *Wear* **2000**, *241*, 193–203. [CrossRef]

37. Offner, G. Friction Power Loss Simulation of Internal Combustion Engines Considering Mixed Lubricated Radial Slider, Axial Slider and Piston to Liner Contacts. *Tribol. Trans.* **2013**, *56*, 503–515. [CrossRef]

38. Westerfield, Z.; Totaro, P.; Kim, D.; Tian, T. *An Experimental Study of Piston Skirt Roughness and Profiles on Piston Friction Using the Floating Liner Engine*; SAE International: Warrendale, PA, USA, 2016.

39. Mufti, R.A.; Priest, M. Experimental and Theoretical Study of Instantaneous Engine Valve Train Friction. *J. Tribol.* **2003**, *125*, 628–637. [CrossRef]

40. Marušić-Paloka, E.; Pažanin, I. Effects of boundary roughness and inertia on the fluid flow through a corrugated pipe and the formula for the Darcy-Weisbach friction coefficient. *Int. J. Eng. Sci.* **2020**, *152*, 103293. [CrossRef]

41. Moody, L.F. Approximate formula for pipe friction factors. *Mech. Eng.* **1947**, *69*, 1005–1011.

42. Wang, T.T.; Jagarwal, A.; Wagner, J.R.; Fadel, G. Optimization of an automotive radiator fan array operation to reduce power consumption. *IEEE ASME Trans. Mechatronics* **2014**, *20*, 2359–2369. [CrossRef]

43. Teodorescu, M.; Taraza, D.; Henein, N.A.; Bryzik, W. Simplified Elasto-Hydrodynamic Friction Model of the Cam-Tappet Contact. *SAE Tech. Pap. Ser.* **2003**. [CrossRef]

44. Guo, J.; Zhang, W.; Zou, D. Investigation of dynamic characteristics of a valve train system. *Mech. Mach. Theory* **2011**, *46*, 1950–1969. [CrossRef]

45. Greenwood, J.A.; Williamson, J.B.P. Contact of nominally flat surfaces. *Proc. R. Soc. London. Ser. A Math. Phys. Sci.* **1966**, *295*, 300–319. [CrossRef]

46. Sadeghi, F.; Slack, T. *Handbook of Lubrication and Tribology*; CRC Press: Boca Raton, FL, USA, 2012; Volume II. [CrossRef]

47. Goksem, P.G.; Hargreaves, R.A. The Effect of Viscous Shear Heating on Both Film Thickness and Rolling Traction in an EHL Line Contact—Part I: Fully Flooded Conditions. *J. Lubricants Technol.* **1978**, *100*, 346–352. [CrossRef]

48. Dowson, D.; Higginson, G.R. *Elasto-Hydrodynamic Lubrication*; Pergamon: Oxford, UK, 1977.

49. Menacer, B.; Bouchetara, M. The compression ring profile influence on hydrodynamic performance of the lubricant in diesel engine. *Adv. Mech. Eng.* **2020**, *12*, 168781402093084. [CrossRef]

50. Delprete, C.; Razavykia, A.; Baldissera, P. Detailed analysis of piston secondary motion and tribological performance. *Int. J. Engine Res.* **2020**, *21*, 1647–1661. [CrossRef]

51. Jang, S.; Cho, J. Effects of skirt profiles on the piston secondary movements by the lubrication behaviors. *Int. J. Automot. Technol.* **2004**, *5*, 23–31.

52. Delprete, C.; Razavykia, A. Piston dynamics, lubrication and tribological performance evaluation: A review. *Int. J. Engine Res.* **2020**, *21*, 725–741. [CrossRef]

53. Jeng, Y.-R. Theoretical Analysis of Piston-Ring Lubrication Part I—Fully Flooded Lubrication. *Tribol. Trans.* **1992**, *35*, 696–706. [CrossRef]

54. Greenwood, J.A.; Tripp, J.H. The Contact of Two Nominally Flat Rough Surfaces. *Proc. Inst. Mech. Eng.* **1970**, *185*, 625–633. [CrossRef]

55. Teodorescu, M.; Balakrishnan, S.; Rahnejat, H. Integrated Tribological Analysis within a Multi-physics Approach to System Dynamics. *Tribol. Metal Cutt.* **2005**, *48*, 725–737. [CrossRef]

56. Taylor, C. Engine tribology. *Tribol. Int.* **1997**, *30*, 464–465. [CrossRef]

57. Internal combustion engine fundamentals. *Choice Rev. Online* **1988**, *26*, 26. [CrossRef]

58. Nikolakopoulos, P.G.; Mavroudis, S.; Zavos, A. Lubrication Performance of Engine Commercial Oils with Different Performance Levels: The Effect of Engine Synthetic Oil Aging on Piston Ring Tribology under Real Engine Conditions. *Lubricants* **2018**, *6*, 90. [CrossRef]